ORIGINAL RESEARCH

Histone Methyltransferase Dot1L Contributes to RIPK1 Kinase-Dependent Apoptosis in Cerebral Ischemia/Reperfusion

Jinghuan Wang (iD), PhD; Wen Zhong, BS; Haibi Su, BS; Jie Xu, BS; Di Yang, PhD; Xinhua Liu (iD), PhD; Yi Zhun Zhu, PhD

BACKGROUND: Neuron apoptosis is a pivotal process for brain damage in cerebral ischemia. Dot1L (disruptor of telomeric silencing 1-like) is only known histone H3K79 methyltransferase. It is not clear whether the role and mechanism of Dot1L on cerebral ischemia is related to regulate neuron apoptosis.

METHODS AND RESULTS: We use a combination of mice middle cerebral artery occlusion stroke and neurons exposed to oxygen-glucose deprivation followed by reoxygenation to investigate the role and mechanism of Dot1L on cerebral ischemia. We find knockdown or inhibition of Dot1L reversed ischemia-induced neuronal apoptosis and attenuated the neurons injury treated by oxygen-glucose deprivation followed by reoxygenation. Further, blockade of Dot1L prevents RIPK1 (receptor-interacting protein kinase 1)-dependent apoptosis through increased RIPK1 K63-ubiquitylation and decreased formation of RIPK1/Caspase 8 complexes. In line with this, H3K79me3 enrichment in the promoter region of deubiquitin-modifying enzyme A20 and deubiquitinase cylindromatosis gene promotes the increasing expression in oxygen-glucose deprivation followed by reoxygenation -induced neuronal cells, on the contrary, oxygen-glucose deprivation followed by reoxygenation decreases H3K79me3 level in the promoter region of ubiquitin-modifying enzyme cIAP1 (cellular inhibitors of apoptosis proteins), and both these factors ultimately cause K63-deubiquitination of RIPK1. Importantly, knockdown or inhibition of Dot1L in vivo attenuates apoptosis in middle cerebral artery occlusion mice and reduces the extent of middle cerebral artery occlusion -induced brain injury.

CONCLUSIONS: These data support for the first time, to our knowledge, that Dot1L regulating RIPK1 to the apoptotic death trigger contributes to cerebral ischemia injury. Therefore, targeting Dot1L serves as a new therapeutic strategy for ischemia stroke.

Key Words: cIAP ■ CYLD ■ Dot1L ■ middle cerebral artery occlusion ■ oxygen-glucose deprivation ■ RIPK1

Stroke is a major cause of disability and mortality around the world.[1] At present, the most important treatment for ischemic stroke is to restore the blood supply quickly, which are believed to replenish nutrients and oxygen, as well as remove toxic metabolites. However, restoration of blood flow might also aggravate brain injury and functional damage, resulting in cerebral ischemia-reperfusion injury (I/R). Many studies have proven several mechanisms involved in the pathological process of I/R injury, including excitatory toxicity, oxidative stress, inflammation, and apoptosis.[2,3] Hence, prevention of apoptosis and restoration of blood flow are among the most important strategies, which could be a target for treatment of ischemic stroke.

The extrinsic pathway of apoptosis is initiated by the binding of death ligands of the TNF receptor

---

CLINICAL PERSPECTIVE

What Is New?

- Using oxygen glucose deprivation-induced primary cortical neurons and disruptor of telomeric silencing 1-like (Dot1L) knockdown mice subjected to middle cerebral artery occlusion, we determine histone H3K79 methyltransferase Dot1L participates in cerebral ischemic diseases.
- Blockade of Dot1L prevents neurons from initiating apoptosis and promotes restoration of blood flow and provides neuroprotection against cerebral ischemia.

What Are the Clinical Implications?

- Our study reveals a previously unexplored role for Dot1L in cerebral ischemia disease, suggesting that Dot1L may represent a novel opportunity for the therapeutic manipulation of ischemic stroke.

Nonstandard Abbreviations and Acronyms

Dot1L	Disruptor of telomeric silencing 1-like
Dot1L$^{+/-}$	Dot1L heterozygous knockout
I/R	ischemia-reperfusion injury
MCAO	middle cerebral artery occlusion
OGD/R	oxygen-glucose deprivation followed by reoxygenation
WT	wild-type

superfamily.[4] Ligation of TNF (tumor necrosis factor) to TNFR1 (tumor necrosis factor receptor-1) results in formation of a membrane protein complex (called Complex I). RIPK1 (receptor-interacting protein kinase 1), a protein of the receptor-interacting protein kinase family, is ubiquitinated in Complex I to induce the formation of a cell survival complex that promotes activation of nuclear factor-κB.[5,6] The cIAP (cellular inhibitors of apoptosis proteins) 1/2 maintain RIPK1 in this complex to decrease the release of RIPK1 from this complex. But the degradation of cIAP1/2 would promotes the deubiquitination of RIPK1 by deubiquitinase cylindromatosis (CYLD) releases RIPK1 from this complex and results in the interaction of RIPK1 with FADD (Fas-associated death domain protein), RIPK3, and Caspase 8 to form a cytosolic protein complex (Complex II), leading to the activation of Caspase 8.[7,8] Activated Caspase 8 can cleave and activate the executor caspases such as Caspase 3 and Caspase 7. This in turn triggers downstream effector mechanisms of apoptosis.

In recent years, mounting evidence indicates that aberrant histone modification patterns can play a causative role in disease. Since epigenetic alterations are reversible in nature, histone (de) modifiers are attractive therapeutic targets.[9] Dot1L (disruptor of telomeric silencing 1-like) is a histone H3K79 methyltransferase and produces mono-, di-, and tri-methylated histone H3 lysine 79 (H3K79me1/2/3).[10] Recent genome-wide analysis of the mammalian epigenome has shown that H3K79 methylation is mainly associated with actively transcribed genes.[11,12] Dot1L involved in the control of gene expression further supports the relationship between H3K79 methylation and gene expression.[13–15] Earlier studies have reported that Dot1L plays an important role in heart embryonic growth and cell cycle,[16] telomeric silencing, and the DNA damage response.[17] Histone modifications mediate gene expression, therefore, significantly influence functional outcome and neuronal survival after cerebral ischemia.[18] Nevertheless, it remains unclear whether Dot1L participates in cerebral ischemic diseases. Understanding the regulatory effect of Dot1L could not only uncover additional therapeutic opportunities, but also provide information about the fundamental function of Dot1L and H3K79 methylation in mammalian gene regulation.

In the present study, we discover Dot1L-mediated cell death and inflammatory responses in cerebral I/R injury. Importantly, knockdown or inhibition of Dot1L mice is protected from I/R injury and also promotes better recovery after stroke. Importantly, we find that deubiquitinase A20 and CYLD and ubiquitinase cIAP1, as crucial factors for the activation of RIPK1/Caspase 8 signaling in apoptosis, are the target genes of Dot1L. The results of this study expand our knowledge in the molecular mechanisms of Dot1L contributing to RIPK1 kinase-dependent apoptosis and demonstrate that blockade of Dot1L provides neuroprotection against cerebral ischemia.

METHODS

The data that support the finding of this study are available within the article and in Data S1.

Experimental Animals

All animals and the experimental protocol conformed to the Animal Welfare Act Guide for Use and Care of Laboratory Animals and were approved by Institutional Animal Care and Use Committee, Fudan University, China. To investigate the role of Dot1L on neuroprotection in vivo, Dot1L heterozygous knockout (Dot1L$^{+/-}$) mice were generated on a C57BL/6J background by using CRISPR/Cas9 system, for the sake of homozygous deletion of Dot1L led to embryonic lethality.

Cell Culture

Primary cortical neurons were obtained from SD (Sprague Dawley) rats after birth day 1 as previously described[19] and cultured at 37 °C in DMEM containing 10% fetal bovine serum (Gibco, USA). After 8 hours, the medium was changed into fetal bovine serum-free DMEM-F12 (Hyclone, USA) medium containing 2% B27. Cells were cultured for 7 days and were identified using specific neuron marker Map-2 (Microtubule-associated Protein 2) by immunofluorescent staining.

Oxygen-Glucose Deprivation Model in Vitro

Oxygen-glucose deprivation followed by reoxygenation (OGD/R) was established as follows: The prepared neurons were cultured in DMEM glucose-free medium and were incubated for 4 hours in <0.1% oxygen in the hypoxia box. Then cultures were switched to completely normal conditions for 24 hours.

RNA Extraction and Quantitative Real-Time Polymerase Chain Reaction

Total RNA was isolated from the cells or tissues using TRIzol reagent (Takara Bio Inc., China). Reverse transcription was performed according to the instruction of the Prime RT Master Mix kit (Takara Bio Inc., China). Quantitative real-time polymerase chain reaction was performed in triplicate using SYBR Premix EX Taq II (Yeasen Biotech Co., Ltd. China). The sequences of primers were shown in Table S1.

Statistical Analysis

Data were expressed as mean±SD. Differences of means were analyzed by using 1-way ANOVA with the Tukey–Kramer post hoc test for multiple groups, and when comparing between 2 groups using unpaired Student t-tests. $P < 0.05$ was accepted as statistically significant.

RESULTS

Dot1L Expression at Different Time Points After OGD in Cultured Cortical Neurons and After Middle Cerebral Artery Occlusion

Time course experiments clearly showed that the level of Dot1L and H3K79me3 was elevated at 1 hour after OGD in the primary cortical cultures (Figure S1A). OGD also induced mRNA expression of Dot1L (Figure S1B). To examine whether Dot1L contributes to damage after stroke, mice were subjected to 90-minutes middle cerebral artery occlusion (MCAO) followed by 24 hours reperfusion. In line with the findings of in vitro OGD,

we observed that the level of Dot1L was increased after MCAO; brain tissue from MCAO mice exhibited an increase in H3K79me3 abundance (Figure S1C). Therefore, we next determined the contribution of Dot1L to the cerebral I/R injury.

Inhibition of Dot1L Reduces Infarct Volume and Neuronal Apoptosis After MCAO

EPZ5676, a specific inhibitor of Dot1L, was used to investigate the effects on MCAO mice. The design of the experiment was shown in Figure 1A. Firstly, we determined the content of EPZ5676 in brain tissue and plasma by HPLC (High Performance Liquid Chromatography) method, and found concentrations reached to certain level in serum and brain tissue, respectively (Figure 1B). Compared with the MCAO group, using EPZ5676 reduced infarct volume and Bederson score after MCAO (Figure 1C and 1D). After MCAO, the level of cell apoptosis was higher in vehicle treated-mice brain sections relative to EPZ5676-treated mice brain sections (Figure 1E). Further, our results revealed that cleaved-Caspase 3, cleaved-Caspase 9, cleaved-PARP1, p53, and Bax (BCL2-associated X protein) protein were induced by I/R injury, anti-apoptotic factor Bcl-2 was downregulated in these same samples, however, the altered regulation of these genes was markedly attenuated in brain tissues from EPZ5676-treated mice (Figure 1F). There is now strong evidence that inflammatory processes may contribute to secondary brain damage after ischemic stroke.[20] Consistently, EPZ5676 also decreased the expression of proinflammatory cytokines including VCAM-1 (Vascular Cell Adhesion Molecule-1), COX-2 (Cyclooxygenase-2), iNOS (Inductible Nitric Oxide Synthase) in the MCAO mice (Figure 1F). Breakdown of the blood-brain barrier has been reported in stroke pathology. The decrease of tight junction proteins ZO-1 (Zonula Occluden-1) and Claudin-1 in the penumbra of MCAO was reversed by EPZ5676 (Figure 1F). Double immunofluorescence staining with neuron marker Map-2 further showed EPZ5676 inhibited pro-apoptosis and inflammation protein level in neurons after MCAO (Figure 1G and Figure S2). Also, the images of double immunofluorescence staining with ZO-1 and CD31 (an endothelial cell marker) further showed the level of ZO-1 significantly was increased after treatment with EPZ5676 (Figure 1G). These results suggest that EPZ5676 inhibits the activation of apoptotic initiators and inflammation response, and then reduces infarct volume.

Dot1L Knockdown Mice Are More Resistant to Focal Cerebral Ischemia

To investigate the role of Dot1L on neuroprotection in vivo, wild-type (WT) and Dot1L^{+/-} mice were subjected
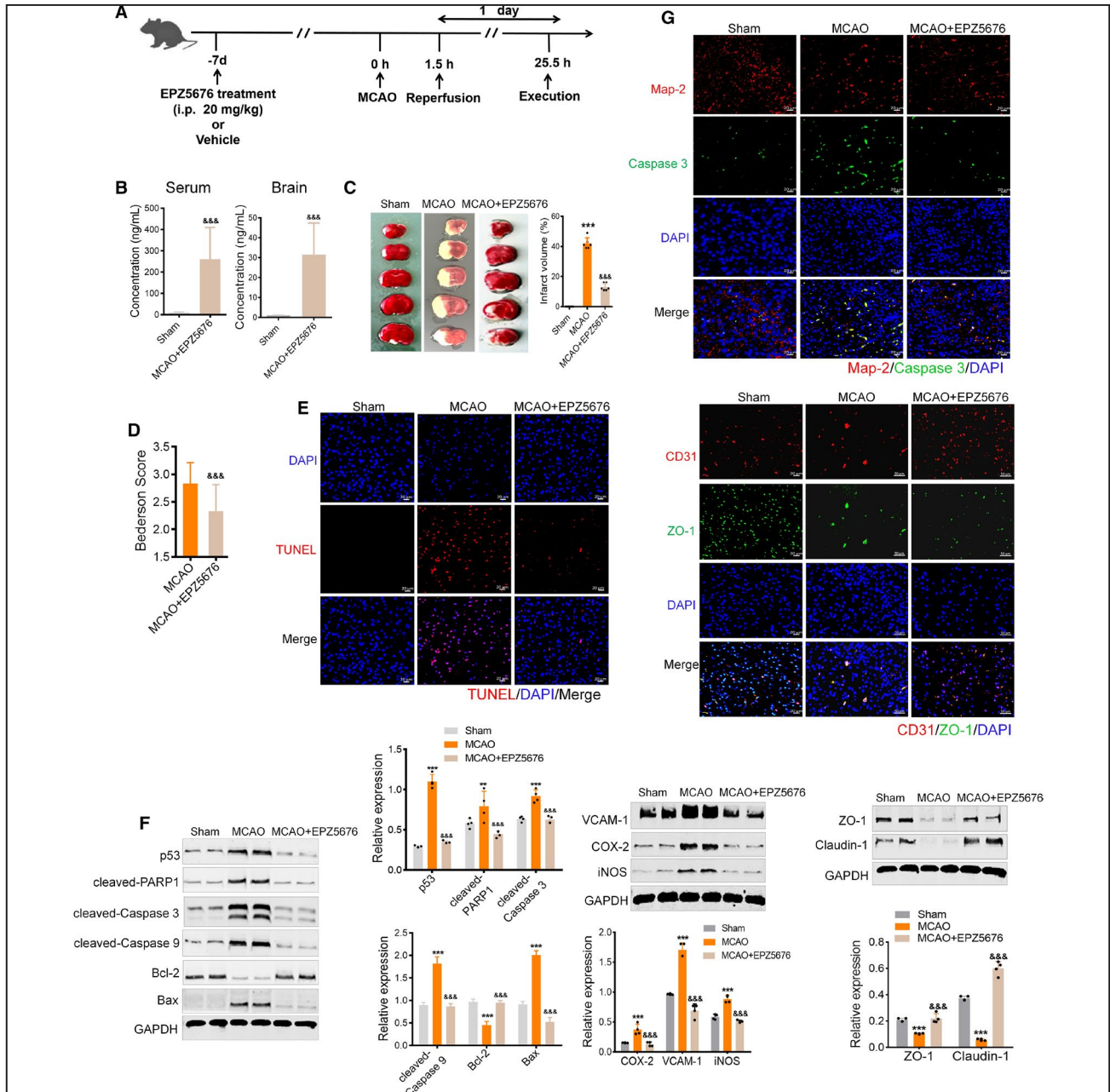
Figure 1. Inhibition of Dot1L (disruptor of telomeric silencing 1-like) reduces infarct volume and neuronal apoptosis after middle cerebral artery occlusion (MCAO).

A, Experimental scheme. Mice required EPZ5676 treatment for 1 weeks before MCAO for 90 minutes, then brains are harvested 24 hours after MCAO injury. **B**, The contents of EPZ5676 in brain tissue and blood after MCAO were detected by high performance liquid phase. Data are presented as mean±SD, n=6, $^{\&\&\&}P<0.001$ compared with Sham group. **C**, TTC (2,3,5-Triphenyltetrazolium chloride) staining was performed to show the ischemic regions. Data are presented as mean±SD, n=6, $^{***}P<0.001$ compared with Sham group, $^{\&\&\&}P<0.001$ compared with MCAO group. **D**, The neurological deficit scores of mice after MCAO. Data are presented as mean±SD, n=6, $^{\&\&\&}P<0.001$ compared with MCAO group. E, The apoptosis of neurons was evaluated by TUNEL. Scale bars: 20 μm. DAPI, 4,6-diamino-2-phenyl indole; Map, Microtubule-associated Protein; VCAM, Vascular Cell Adhesion Molecule; iNOS, Inductible Nitric Oxide Synthase; PARP, Poly (ADP-ribose) polymerase. F, Immunoblot analysis of apoptosis-related proteins (Bax, BCL2-associated X protein; Bcl-2, p53, cleaved-PARP1, cleaved-Caspase 3, cleaved-Caspase 9), inflammation markers (iNOS, VCAM-1, COX-2), and tight junction-associated proteins (Claudin-1, ZO-1) in brain of mice after MCAO. Data shown are presented as mean±SD from at least 4 independent replicates for 6 to 10/group, $^{**}P<0.01$, $^{***}P<0.001$ compared with Sham group, $^{\&\&\&}P<0.001$ compared with MCAO group. The data are analyzed and counted through T-test. COX, Cyclooxygenase; PARP, Poly (ADP-ribose) polymerase 1; Bcl-2, B-cell lymphoma-2; GAPDH, Glyceraldehyde-3phosphate dehydrogenase; ZO, Zonula Occluden. G, Immunofluorescence staining of Map-2 and Caspase 3 or CD31 and ZO-1 in brain of mice after MCAO. Scale bars: 20 μm. MCAO indicates middle cerebral artery occlusion; and TUNEL, terminal deoxynucleotidal transferase–mediated biotin–deoxyuridine triphosphate nick-end labeling.

to 90-minutes MCAO followed by 24 hours reperfusion. Initially, Western blot determined that Dot1L levels remained low in the brains of Dot1L^{+/-} mice compared with the WT mice (Figure S3A). 2,3,5-Triphenyltetrazolium chloride-staining image and quantitative analysis of brain infarction indicated that knockdown of Dot1L led to smaller infarct size compared with the WT mice (Figure 2A). Likewise, compared with the WT-MCAO mice, Dot1L^{+/-}-MCAO mice improved functional outcome, as assessed by the Bederson score (Figure 2B). Blood-brain barrier permeability was evaluated by the Evans blue staining in the brains and found leaked Evans blue in Dot1L^{+/-}-MCAO mice was significantly reduced compared with WT-MCAO mice (Figure 2C). Meanwhile, the knockdown Dot1L resulted in a significant increase in cerebral blood flow compared with WT at 24 hours reperfusion (Figure 2D). The TUNEL (terminal deoxynucleotidal transferase–mediated biotin–deoxyuridine triphosphate nick-end labeling) staining showed that lacking Dot1L decreased the number of apoptotic cells in mice brain tissue after MCAO (Figure 2E). No obvious change was observed between WT-Sham and Dot1L^{+/-}-Sham in the above experiments. These results show knockdown of Dot1L decreased MCAO-induced brain infarct volume and brain tissue damage and improved behavioral outcomes.

Knockdown Dot1L Reduces Apoptosis and Inflammation Response

Considering the neuropathogenesis after reperfusion is generally associated with neural cell apoptosis, we further assessed the role of Dot1L knockdown in regulating neural cell apoptosis. We observed that the level of Dot1L was increased after MCAO (Figure 3A). Furthermore, knockdown Dot1L reversed the upregulation of pro-apoptotic gene in I/R mice brain tissues, whereas it enhanced the expression of anti-apoptotic factor Bcl-2 in these same samples (Figure 3A). Notably, immunofluorescence staining analyses revealed that positive Caspase 3 staining was localized to Map-2-positive neuron in the cerebral cortex after MCAO injury, Caspase 3 expression was markedly attenuated in Dot1L^{+/-}-MCAO mice brain tissues relative to those from WT-MCAO (Figure 3B). Meanwhile, MCAO-induced upregulated protein levels of iNOS, COX-2, and VCAM-1 were inhibited by knockdown Dot1L (Figure 3C). Dot1L^{+/-}-MCAO mice brain tissues section showed a small degree of immunostaining for iNOS compared with WT-MCAO mice (Figure 3D). Immunofluorescence staining further determined knockdown Dot1L resulted in the reduction of iNOS and COX-2 expressions in neurons in penumbra after MCAO (Figure S3B). We also investigated the effects of knockdown Dot1L on the expression of ZO-1 and Claudin-1 at 24 hours after reperfusion and found knockdown Dot1L could upregulate

the expressions of ZO-1 and Claudin-1 after ischemic stroke in mice (Figure 3E and 3F). mRNA expressions of *p53, Cox-2*, *CLDN1*, and *Tjp1* are consistent with protein expression trends that the altered regulation of these genes was markedly attenuated in Dot1L^{+/-}-MCAO mice brain tissues relative to those from WT-MCAO mice (Figure S3C). These results demonstrate knockdown of Dot1L reduced apoptosis and inflammation response and upregulated the expression of tight junction proteins following I/R.

Suppression or Knockdown of Dot1L Reduces Neuronal Apoptosis and Inflammation Response After OGD

We first investigated the effect of EPZ5676 in neuron subjected to 4 hours of OGD and 24 hours reoxygenation. EPZ5676 with a concentration-dependent manner reversed the upregulation of pro-apoptotic gene and inflammation modulators induced by OGD/R in neuron, whereas enhanced the expression of anti-apoptotic factor Bcl-2 in these same samples (Figure 4A). Immunofluorescence analyses revealed that positive Caspase 3 staining was inhibited by EPZ5676 (Figure 4B). Notably, OGD/R-induced neuron apoptosis was significantly recovered by the pretreatment with EPZ5676 (Figure 4C). Consistent with these findings, immunofluorescence staining revealed a lack of iNOS and VCAM-1 in EPZ5676 treated neuron as compared with those in OGD/R-treated neuron (Figure S4A). Likewise, mRNA expression in apoptosis markers (p53, Bax), and inflammation markers (Nos2, Cox-2, and Vcam-1) were consistent with protein expression (Figure S4B). These results provide further support that EPZ5676 protects against cortical neuron OGD/R injury.

To further determine the effect of Dot1L on OGD/R-treated neurons, we used siRNA to knock down Dot1L. When Dot1L was knocked down, cortical neurons subjected to OGD/R exhibited a decrease in H3K79me3 abundance (Figure 4D). In addition, pro-apoptotic gene and inflammation modulators induced by OGD/R could be inhibited by knockdown Dot1L (Figure 4E). The knockdown of Dot1L also attenuated neuronal death after OGD by TUNEL assay (Figure 4F). Similarly, immunofluorescence assay further confirmed that silencing of Dot1L decreased p53 and COX-2 expression (Figure S4C). These observations demonstrate that in vitro as well as in vivo, Dot1L contributes to ischemia damage.

Blockade of Dot1L Promotes K63-Linked Ubiquitination of RIPK1 to Inhibit RIPK1/ Caspase 8-Dependent Apoptosis Pathway

Receptor-interacting protein kinase 1 (RIPK1, also known as RIP1) and Caspase 8 are key players in
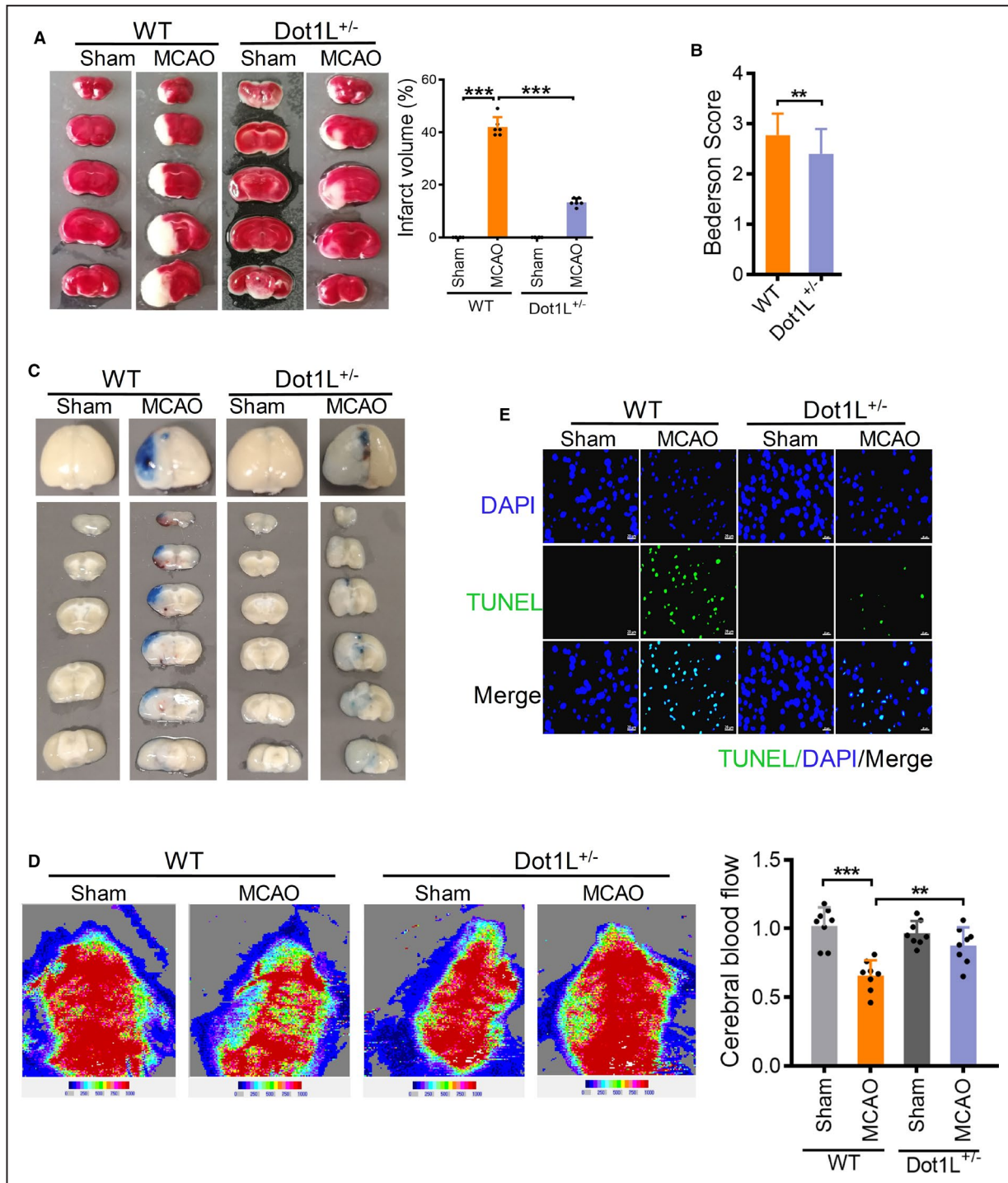
Figure 2. Mice lacking Dot1L (disruptor of telomeric silencing 1-like) reduces ischemia-reperfusion–induced-brain infarct volume and edema and improved behavioral outcomes.

Wild-type and Dot1L heterozygous knockout mice were subjected to 90-minutes middle cerebral artery occlusion followed by 24 hours reperfusion. **A**, TTC (2,3,5-Triphenyltetrazolium chloride) staining was performed to show the ischemic regions. **B**, The neurological deficit scores of mice after middle cerebral artery occlusion. **C**, Representative images of Evans blue leakage in each group at 24 hours of reperfusion after middle cerebral artery occlusion. **D**, Relative change in cerebral blood flow was assessed 24 hours of reperfusion after middle cerebral artery occlusion. Data are presented as mean±SD, n=6 to 8/group, [**]$P<0.01$, [***]$P<0.001$. The data are analyzed and counted through ANOVA. **E**, The apoptosis of neurons was evaluated by TUNEL (terminal deoxynucleotidal transferase–mediated biotin–deoxyuridine triphosphate nick-end labeling). Scale bars: 20 μm. Dot1L+/- indicates Dot1L heterozygous knockout; MCAO, middle cerebral artery occlusion; TUNEL, terminal deoxynucleotidal transferase–mediated biotin–deoxyuridine triphosphate nick-end labeling; and WT, wild-type.
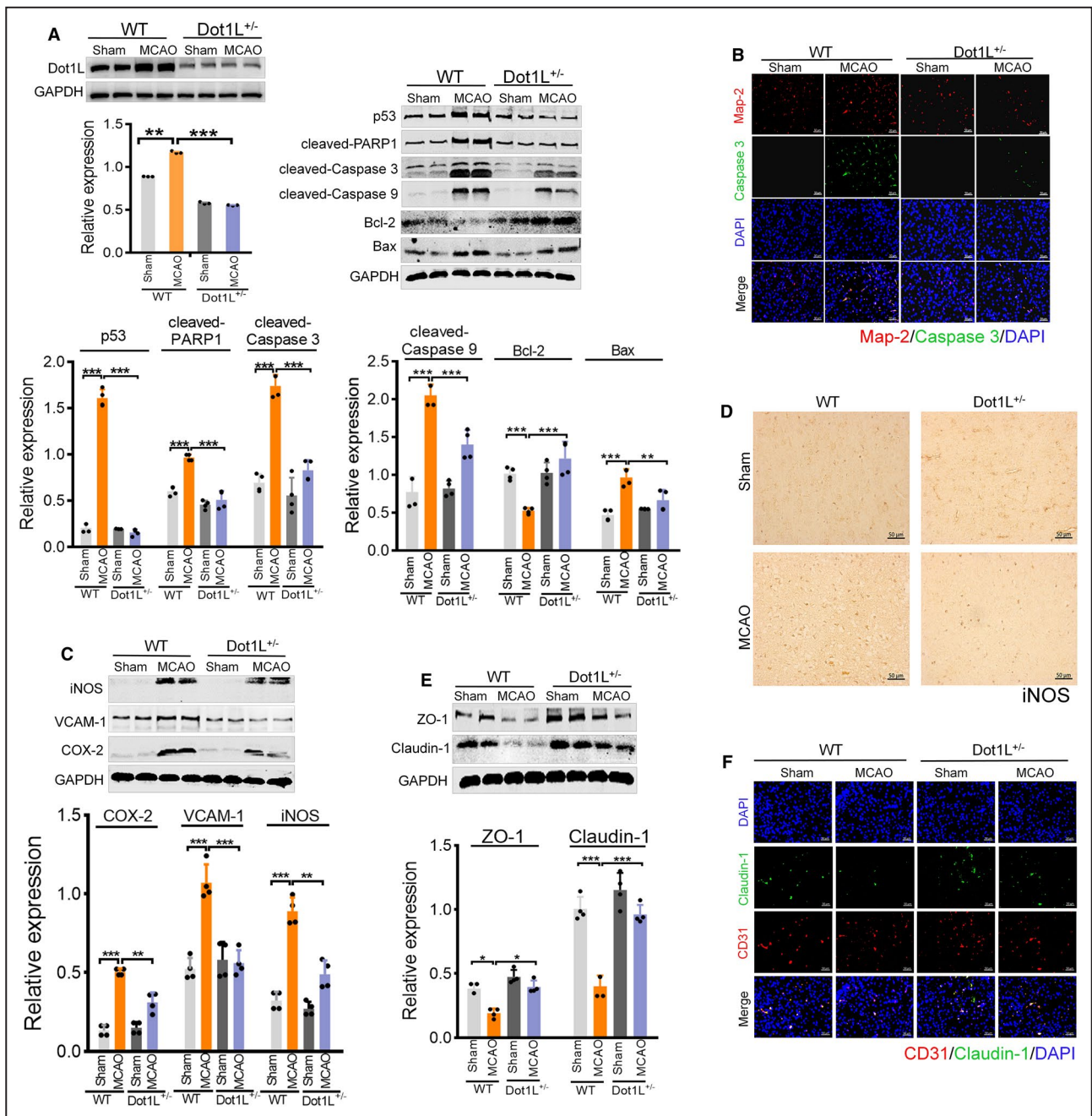
Figure 3. Mice lacking Dot1L (disruptor of telomeric silencing 1-like) reduces apoptosis and inflammation response.
Wild-type and Dot1L heterozygous knockout mice were subjected to 90-minutes middle cerebral artery occlusion (MCAO) followed by 24 hours reperfusion. **A**, Immunoblot analysis of Dot1L and apoptosis-related proteins in brain of mice after MCAO. **B**, Immunofluorescence staining of Map-2 and Caspase 3 in brain of mice after MCAO. Scale bars: 50 μm. **C**, Immunoblot analysis of inflammation markers in brain of mice after MCAO. **D**, Immunohistochemistry staining of iNOS in brain of mice after MCAO. Scale bars: 50 μm. **E**, Immunoblot analysis of TJs-associated proteins in brain of mice after MCAO. **F**, Immunofluorescence staining of CD31 and Claudin-1 in brain of mice after MCAO. Scale bars: 50 μm. All blots data shown are presented as mean±SD from at least 4 independent replicates for 6 to 10/group, $^*P<0.05$, $^{**}P<0.01$, $^{***}P<0.001$. The data are analyzed and counted through ANOVA. Bax, BCL2-associated X protein; Bcl, B-cell lymphoma; COX, Cyclooxygenase; DAPI, 4,6-diamino-2-phenyl indole; GAPDH, Glyceraldehyde-phosphate dehydrogenase; iNOS, Inductible Nitric Oxide Synthase; Map, Microtubule-associated Protein; PARP, Poly (ADP-ribose) polymerase; VCAM, Vascular Cell Adhesion Molecule; ZO, Zonula Occluden. Dot1L+/- indicates Dot1L heterozygous knockout; MCAO, middle cerebral artery occlusion; TUNEL, terminal deoxynucleotidal transferase–mediated biotin–deoxyuridine triphosphate nick-end labeling; and WT, wild-type.
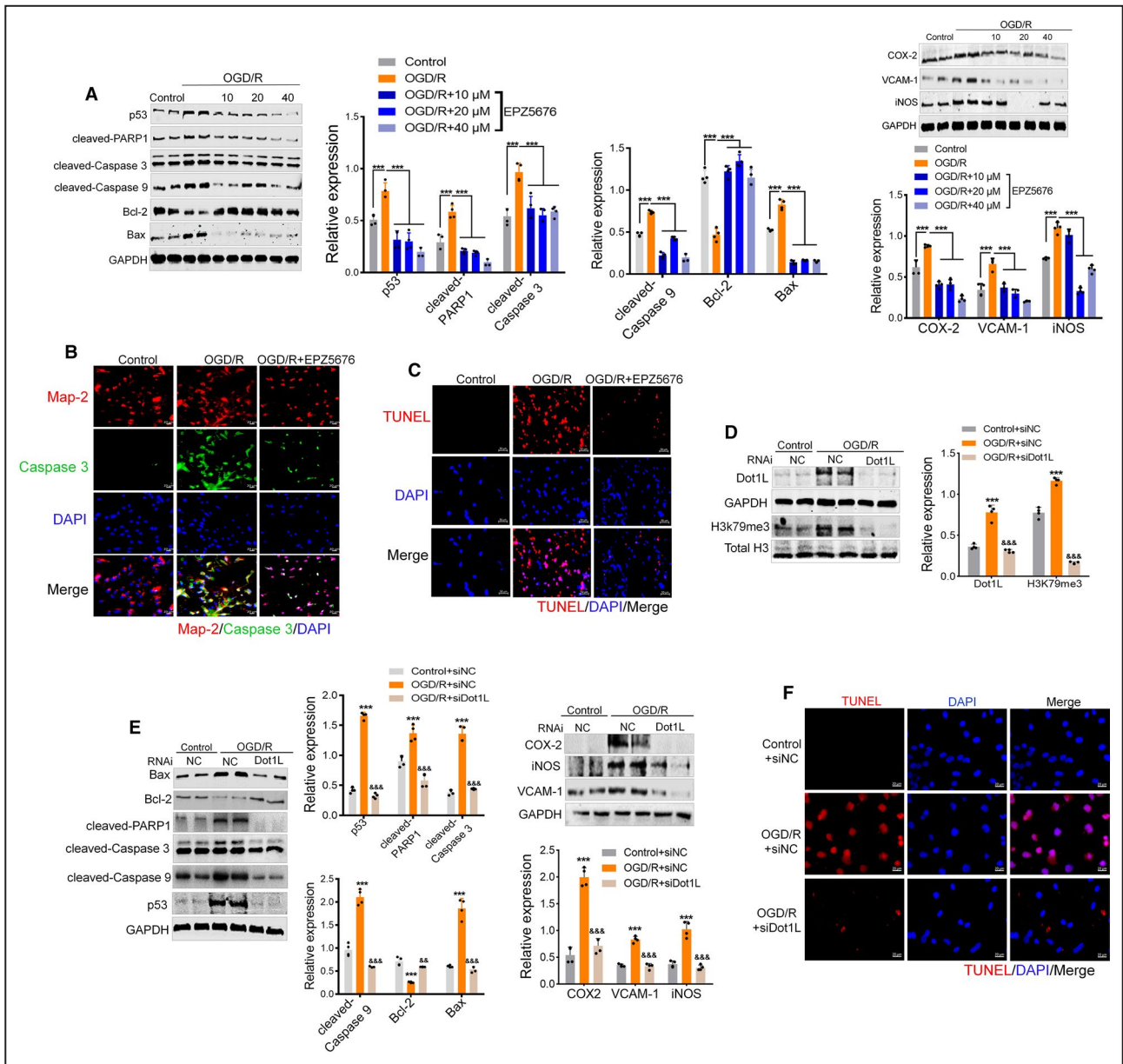
Figure 4. **Suppression or knockdown of Dot1L (disruptor of telomeric silencing 1-like) reduces neuronal apoptosis and inflammation response after oxygen-glucose deprivation (OGD).**

Rat neocortical neurons were pretreated with EPZ5676 (10, 20, 40 µmol/L) for 4 hours and subsequently treated with OGD 4 hours and 24 hours of reoxygenation. Immunoblot analysis of apoptosis-related proteins and inflammation markers in cortical neurons after OGD (**A**); Immunofluorescence staining of Map-2 and Caspase 3 in cortical neurons after OGD. Scale bars: 20 µm (**B**); The apoptosis of neurons was evaluated by TUNEL (terminal deoxynucleotidal transferase–mediated biotin–deoxyuridine triphosphate nick-end labeling). Scale bars: 50 µm (**C**). Rat neocortical neurons were transfected with either control siRNA (siNC) or Dot1L siRNA cultured for 48 hours and subsequently treated with OGD followed by reoxygenation, immunoblot analysis of Dot1L and H3K79me3 protein expression (**D**) and apoptosis and inflammation markers (**E**); The apoptosis of neurons was evaluated by TUNEL. Scale bars: 20 µm (**F**). All data are presented as mean±SD of 4 independent experiments, $^{***}P<0.001$ compared with control or control+siNC, $^{\&\&}P<0.01$, $^{\&\&\&}P<0.001$ compared with OGD followed by reoxygenation or OGD followed by reoxygenation +siNC. The data are analyzed and counted through ANOVA. OGD/R indicates oxygen-glucose deprivation followed by reoxygenation; and TUNEL, terminal deoxynucleotidal transferase–mediated biotin–deoxyuridine triphosphate nick-end labeling. Bax, BCL2-associated X protein; Bcl, B-cell lymphoma; COX, Cyclooxygenase; DAPI, 4,6-diamino-2-phenyl indole; GAPDH, Glyceraldehyde-phosphate dehydrogenase; iNOS, Inductible Nitric Oxide Synthase; PARP, Poly (ADP-ribose) polymerase; SiNC, negative control siRNA; VCAM, Vascular Cell Adhesion Molecule; ZO, Zonula Occluden.
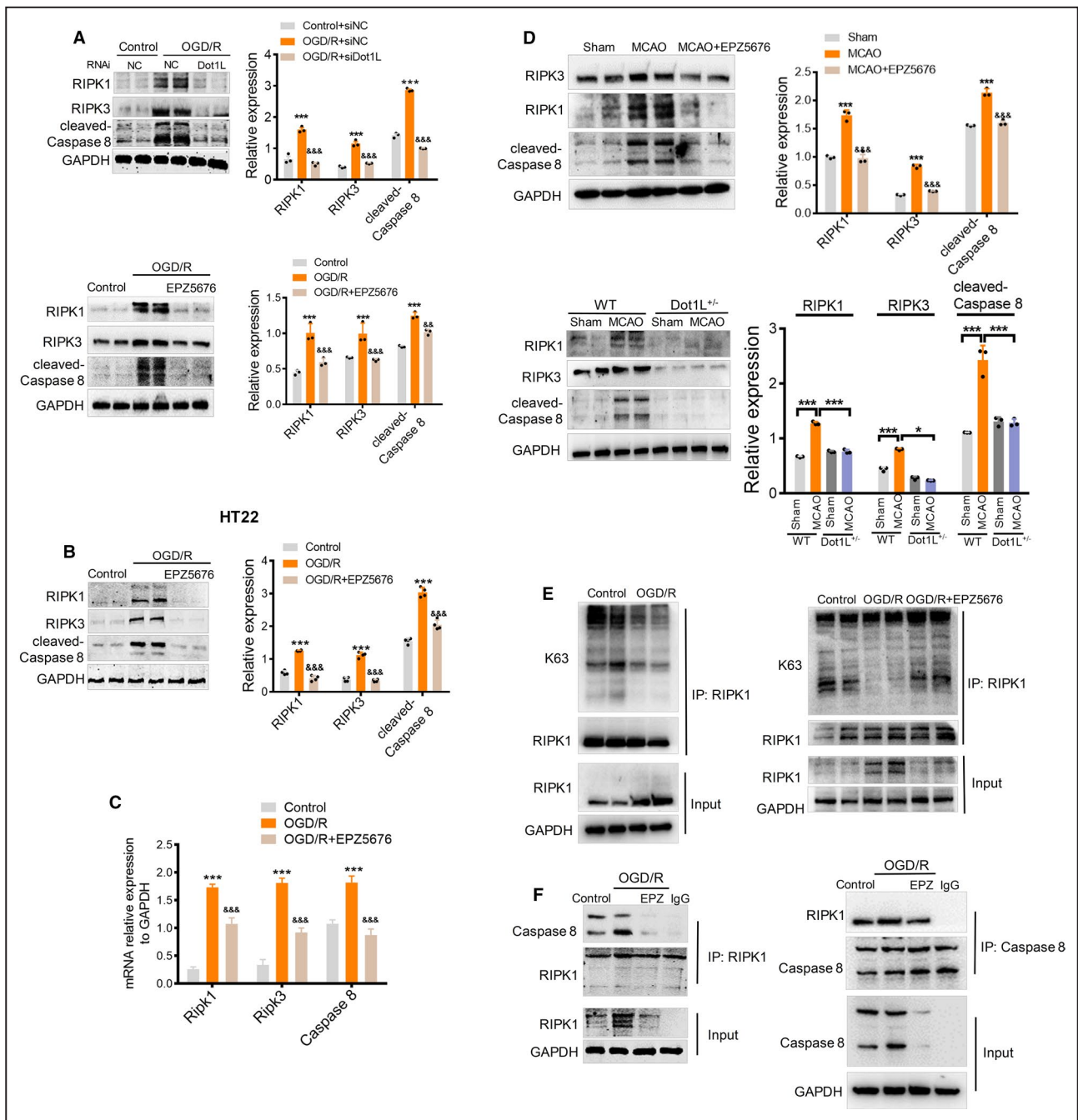
Figure 5. Blockade of Dot1L (disruptor of telomeric silencing 1-like) promotes K63-ubiquitylation of RIPK1 (receptor-interacting protein kinase 1) to inhibit RIPK1/Caspase8-dependent apoptosis pathway.
A, Rat neocortical neurons were transfected with Dot1L siRNA or pretreated with EPZ5676, and subsequently treated with oxygen-glucose deprivation followed by reoxygenation (OGD/R), immunoblot analysis of RIPK1, RIPK3, and cleaved-Caspase 8 expression. HT22 cells were pretreated with EPZ5676 for 4 hours and subsequently treated with OGD/R, immunoblot analysis of RIPK1, RIPK3, and cleaved-Caspase 8 expression (**B**) and quantitative real-time polymerase chain reaction to quantify mRNA level (**C**); Data are presented as mean±SD of 3 independent experiments, ***$P<0.001$ compared with Control or Control+siNC, &&&$P<0.001$ compared with OGD/R or OGD/R+siNC. **D**, Immunoblot analysis of RIPK1, RIPK3 and cleaved-Caspase 8 protein expression in brain of mice after middle cerebral artery occlusion. Data shown are presented as mean±SD from at least 3 independent replicates for 6–10/group, *$P<0.05$, ***$P<0.001$. The data are analyzed and counted through ANOVA. **E**, Blockade of Dot1L enhances the level of K63 chains on RIPK1 compared with OGD/R-treated HT22 cells. **F**, Co-immunoprecipitation experiments show blockade of Dot1L suppressed the interaction of RIPK1 and Caspase 8. Dot1L+/- indicates Dot1L heterozygous knockout; MCAO indicates middle cerebral artery occlusion; OGD/R indicates oxygen-glucose deprivation followed by reoxygenation; RIPK1, receptor-interacting protein kinase 1; RIPK3, receptor-interacting protein kinase 3; WT, wild-type.

inflammation and cell death, positively and negatively regulating these processes depending on the cellular context.[21] In present study, we found OGD/R led to a significant elevation of RIPK1, RIPK3, and cleaved-Caspase 8 protein levels. Importantly, inhibition or RNAi-mediated depletion of Dot1L prevented RIPK1, RIPK3 and cleaved-Caspase 8 protein expression induced by OGD/R in cortical neuronal cells (Figure 5A). HT22 cell, an immortalized mouse hippocampal progenitor cell, is an excellent in vitro model for unveiling the molecular mechanisms of ischemic insults. Hence, by using the HT22 hippocampal mouse cell line, we further unveiled the role of Dot1L. Consistent with the observation in cortical neuron, OGD/R resulted in the upregulation of pro-apoptotic gene in HT22 cells, whereas decreased the expression of anti-apoptotic factors Bcl-2 in these same samples, which can be inhibited by EPZ5676 (Figure S5A). Similarly, immunofluorescence assay further confirmed EPZ5676 decreased p53 expression (Figure S5B). In addition, we demonstrated Caspase 3 activity was decreased sharply in EPZ5676-treated HT22 cells (Figure S5C). Likewise, EPZ5676 prevented protein and mRNA expression of RIPK1, RIPK3 and Caspase 8 induced by OGD/R in HT22 cells (Figure 5B and 5C). Further, treatment with EPZ5676 or knockdown of Dot1L prevented MCAO-induced increase of RIPK1, RIPK3 and cleaved-Caspase 8 (Figure 5D). Those results show that blockade of Dot1L downregulates RIPK1/Caspase 8-dependent apoptosis pathway.

K63-linked ubiquitination of RIPK1 represents a further control point that restricts the lethal potential of RIPK1. In OGD/R-treated HT22 cells, K63-ubiquitination of RIPK1 was reduced and its cleavage increased in complex I, reflective of increased Caspase 8 activity and promote apoptosis, on the contrary, EPZ5676 recovered the decreased K63 chains attached to RIPK1 caused by OGD/R (Figure 5E). Additionally, we analyzed RIPK1/Caspase 8 interactions in HT22 cells and found EPZ5676 prevented formation of Caspase 8/RIPK1 complexes (Figure 5F). Those results show that blockade of Dot1L promotes K63-ubiquitylation of RIPK1, inhibiting RIPK1/Caspase 8-dependent apoptosis pathway.

Dot1L Transcriptionally Activates CYLD and A20, and Inhibits cIAP1 to Promote Complex IIb

cIAP acts as E3 for K63-linked ubiquitination-mediated ubiquitylation of RIPK1, and cIAP1/2-mediated RIPK1 K63 ubiquitination in complex I is believed to prevent the transition of RIPK1 from complex I to complex II.[22] Recent studies have also indicated the formation of a RIPK1-dependent apoptosis-inducing complex (complex IIb), which is formed in the absence of cIAP.[23] A

notion supported by the fact that deubiquitinating enzymes (DUBs) such as CYLD and A20 were suggested to promote complex IIb assembly by dismantling the ubiquitin chains remaining on RIPK1 at complex I.[8,24] Finally, to further investigate whether the protective role of Dot1L inhibition against RIPK1-dependent apoptosis was depending on deubiquitinase and ubiquitinase. We found that OGD/R induced an increased deubiquitinase CYLD and A20 in cortical neurons, but that could be inhibited by either Dot1L siRNA or EPZ5676 (Figure 6A). By contrast, silencing or inhibiting of Dot1L could recover the decreased ubiquitinase cIAP1 upon OGD/R injury (Figure 6A). Similarly, EPZ5676 prevented the altered protein expression of CYLD, A20 and cIAP1 induced by OGD/R in HT22 cells (Figure 6A). The immunostaining of cIAP1 in the OGD/R-treated HT22 cells also showed a decreased expression of cIAP1, which was thus recovered by EPZ5676 treatment (Figure 6B). Similar to the in vitro experiments, ischemia triggered increase of the level of CYLD and A20 and the decrease of cIAP1 in the ischemic cortex after MCAO, nevertheless, the altered regulation of these genes was markedly attenuated in EPZ5676-treated or Dot1L^{+/-} mice brain tissues relative to those from WT or vehicle-treated mice (Figure 6C). As Dot1L is the only methyltransferase targeting H3K79, we performed ChIP assays across the CYLD, A20 and cIAP locus using an anti-H3K79me3 antibody. Remarkably, OGD/R treatment promoted recruitment of H3K79me3 to near the promoter of Cyld (CYLD) and Tnfaip3 (A20) as validated by ChIP-PCR in HT22 cells, instead, OGD/R treatment decreased H3K79me3 level near the promoter of Birc2 (cIAP1) (Figure 6D). Quantitative real-time polymerase chain reaction validated the increased Cyld and Tnfaip3 mRNA abundance, also decreased Birc2 transcription level upon OGD/R treatment, by contrary, the altered regulation of these genes was markedly attenuated by treatment with EPZ5676 (Figure 6D and 6E). In summary, these data suggest that Dot1L transcriptionally activates CYLD and A20 and inhibits cIAP1 via its H3K79 methylation dependent function.

DISCUSSION

The pathogenesis of neuronal damage in the brain after ischemic stroke is highly complex, involving necrotic, apoptotic and autophagic processes. To suppress neuron apoptosis and necrosis, it is essential to elucidate the underlying molecular mechanisms and discover impactful therapeutic target. Epigenetic processes are involved in stroke pathogenesis and recovery, including the deployment of stress responses that modulate cell viability and promote tissue repair and functional reorganization.[25–27] Dot1L is the only known H3K79 methyltransferase and located at the globular domain of nucleosome.[28] Dot1L is broadly known to play roles in the pathogenesis of heart embryonic growth and cell cycle, DNA damage
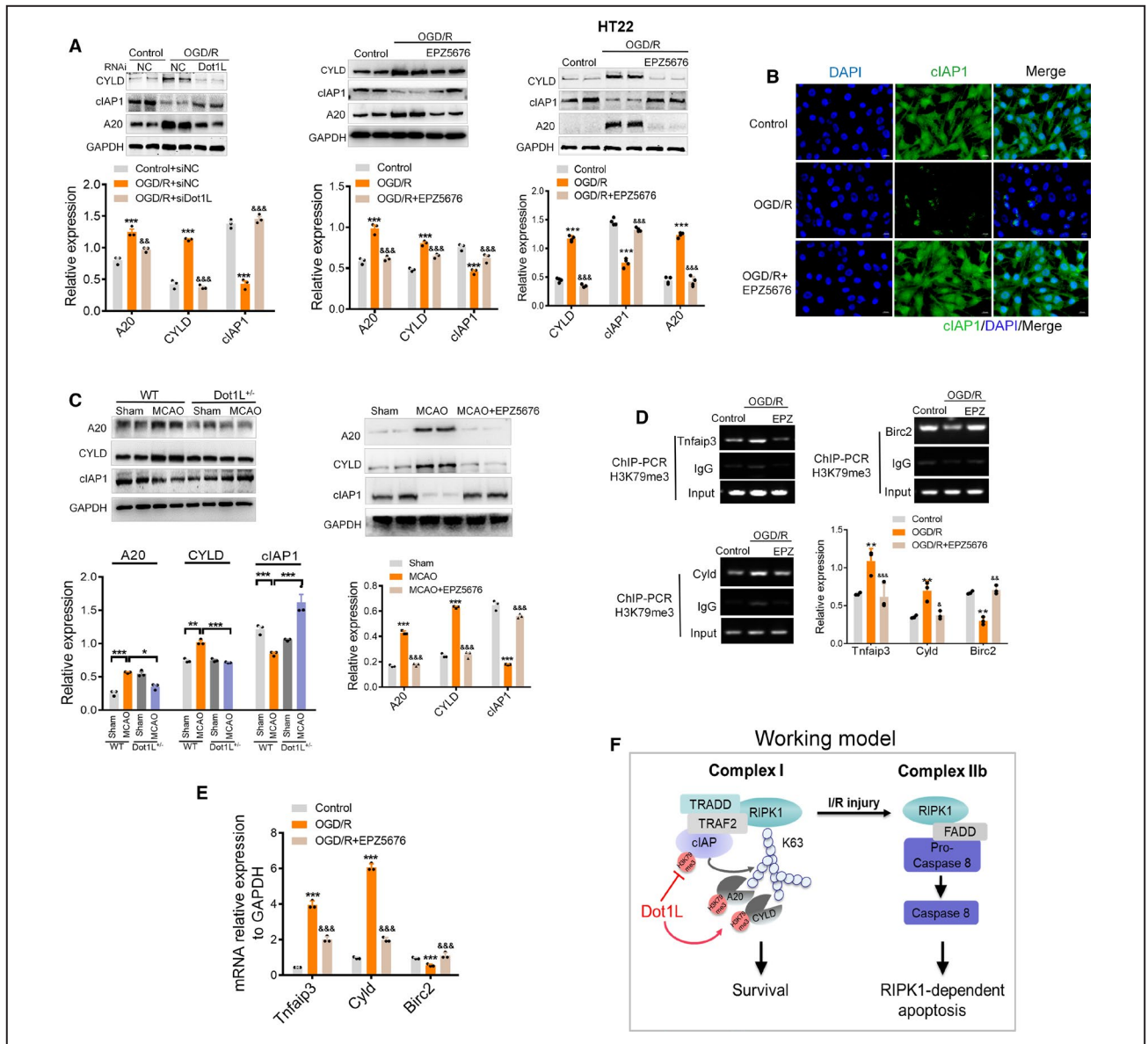
Figure 6. Dot1L (disruptor of telomeric silencing 1-like) transcriptionally activates deubiquitinase cylindromatosis (CYLD) and A20 and inhibits cIAP (cellular inhibitors of apoptosis proteins) to promote complex IIb.

Rat neocortical neurons or HT22 (Hippocampal Neuronal Cell) cells were transfected with Dot1L siRNA or pretreated with EPZ5676, and subsequently treated with oxygen-glucose deprivation followed by reoxygenation (OGD/R), immunoblot analysis of CYLD, A20 and cIAP1 protein expression. Data are presented as mean±SD of 3 independent experiments; ***$P<0.001$ compared with control or control+siNC, &&&$P<0.001$ compared with OGD/R (Oxygen-glucose Deprivation/Reperfusion) or OGD/R+siNC (**A**); Immunofluorescence staining of cIAP1 was assayed. Scale bars: 100 μm (**B**). **C**, Immunoblot analysis of CYLD (Cylindromatosis), A20 and cIAP1 (Cellular Inhibitor Of Apoptosis Protein 1) protein expression in brain of wild-type, Dot1L^{+/-}, EPZ5676-treated mice after middle cerebral artery occlusion. Data shown are presented as mean±SD from at least 3 independent replicates for 6–10/group, *$P<0.05$, **$P<0.01$, ***$P<0.001$ compared with Sham or middle cerebral artery occlusion group, &&&$P<0.001$ compared with middle cerebral artery occlusion group. **D**, ChIP-PCR (Chromatin immunoprecipitation-PCR) showing H3K79me3 lack at promoter of Tnfaip3 and Cyld and gain at promoter of Birc2 in EPZ5676-treated HT22 cells. Data are presented as mean±SD of 3 independent experiments; ***$P<0.01$ compared with Control, &$P<0.05$, &&$P<0.01$, &&&$P<0.001$ compared with OGD/R. **E**, Quantitative real-time polymerase chain reaction to quantify mRNA level of Tnfaip3, Cyld and Birc2 after EPZ5676 treatment in OGD/R-treated HT22 cells. Data are presented as mean±SD of 3 independent experiments, ***$P<0.001$ compared with control, &&&$P<0.001$ compared with OGD/R. The data are analyzed and counted through ANOVA. **F**, Working model for Histone methyltransferase Dot1L contributes to RIPK1 (receptor-interacting protein kinase 1)-dependent apoptosis in cerebral ischemia/reperfusion. Dot1L participates in the regulation of neuronal programmed apoptosis and cerebral infarction through targeting RIPK1/Caspase 8 dependent apoptosis in condition of decreased RIPK1 K63-ubiquitylation obtained by increased CYLD and A20 also cIAP1 depletion. DAPI, 4,6-diamino-2-phenyl indole; GAPDH, Glyceraldehyde-phosphate dehydrogenase; MCAO, Middle Cerebral Artery Occlusion. cIAP1 indicates cellular inhibitors of apoptosis proteins; IgG, immunoglobulin G; MCAO, middle cerebral artery occlusion; OGD/R indicates oxygen-glucose deprivation followed by reoxygenation; RIPK1, receptor-interacting protein kinase 1; TNF, tumor necrosis factor; and WT, wild-type.

response.[11] While the functional role of Dot1L in gene expression regulation has been studied extensively, however, not much is known about Dot1L recruitment to specific sites in regulating programmed apoptosis in the cerebral ischemia. Our present study demonstrated that Dot1L participated in the regulation of neuronal programmed apoptosis and cerebral infarction through targeting RIPK1/Caspase 8 dependent apoptosis in condition of decreased RIPK1 K63-ubiquitylation obtained by increased CYLD (deubiquitinase cylindromatosis) and A20 also cIAP1 depletion (Figure 6F). Importantly, inhibition or knockdown of Dot1L in I/R mice significantly attenuated neurological deficit, decreased brain infarct volume and neuronal apoptosis. Our study has provided important evidence about the function of Dot1L in the programmed apoptosis pathway, a step toward better understanding the Dot1L-based therapy for I/R injury and stroke.

It is well established that apoptosis contributes to neuronal cells death following I/R injury. This was supported by our results wherein transient cerebral ischemia could significantly induce neuron apoptosis, meanwhile, Dot1L is upregulated after cerebral hypoxic-ischemic injury, where Dot1L-mediated apoptosis is assumed to participate. Further studies with a specific inhibitor and knockdown of Dot1L to detect the apoptosis assay are warranted to address this issue. We found that knockdown or inhibition of Dot1L alleviated cell apoptosis in OGD neuronal cells, and significantly attenuated neurological deficit, decreased brain infarct volume and neuronal apoptosis in I/R mice, showing that Dot1L activity contributes to brain I/R injury. It has been demonstrated that an inflammatory response occurs centrally after ischemic injury.[29] Our results also confirmed that ischemic injury induced the increase of inflammation mediators in the brain. Interestingly, Dot1L knockdown or inhibition could simultaneously inhibit inflammatory response in the brain following ischemic stroke and showing blockade of Dot1L may serve as a novel therapeutic strategy for ischemic brain injury.

Covalent conjugation of ubiquitin molecules to target proteins, termed ubiquitination, regulates protein stability and protein-protein interactions in signaling complexes.[30] In particular, K48-linked poly-ubiquitin chains generally target proteins for proteasomal degradation, whereas linear and K63-linked chains primarily serve as a scaffolding network for the formation of signaling complexes.[31,32] The status of RIPK1 K63-ubiquitination determines cell fate by creating either a prosurvival signal (ubiquitinated RIPK1) or a death signal (deubiquitinated RIPK1).[33] When RIPK1 is deubiquitinated, RIPK1 forms a complex with TRADD, FADD, and Caspase 8 to activate Caspase 8 and subsequently trigger apoptosis.[5] This was supported by our results wherein activation of RIPK1 kinase was almost undetectable in sham-operated animals. Transient cerebral ischemia promotes the K63 deubiquitination of RIPK1, and nonubiquitinated RIPK1 binds with Caspase 8 to form complex II and promotes the death receptor pathway of apoptosis. Interestingly, RIPK1/Caspase 8 complex formation is inhibited in Dot1L depletion OGD cells, suggesting that Dot1L might promote RIPK1/Caspase 8 complex formation and activates the apoptotic pathway. However, in dissecting the role of Dot1L in the cell death pathway, we were not able to exclude the role of Dot1L in necroptosis.

It is clear that RIPK1-mediated apoptosis can occur under conditions of IAP (Inhibitor Of Apoptosis Protein) inhibition.[34,35] The overexpression of IAPs can inhibit cell death through ubiquitination of RIPK1. We found K63 ubiquitination level of RIPK1 was reduced upon OGD, in parallel, the expressions of deubiquitinases CYLD and A20 were increased, whilst cIAP1 expression was decreased, which leads to the cleavage and activation of Caspase 8 and the induction of apoptosis. More importantly, an apparent decrease of H3K79me3 signal was shown on promotors of Bric2 (cIAP1) gene in OGD-induced neuronal cells and consequently inhibiting its transcription. Meanwhile, Dot1L initiated H3K79me3 enrichment in the promoter of Cyld and Tnfaip3 (A20) and consequently activated transcription, consistent with Dot1L's methyltransferase activity on H3K79. Taken together, blockade of Dot1L inhibited K63 de-ubiquitination of RIPK1 by downregulated expressions of CYLD and A20, and upregulated cIAP1, thus prevented RIPK1/Caspase 8 complex formation and inhibited apoptotic pathway.

In conclusion, our study was the first to demonstrate that Dot1L was increased in the brain after ischemia, which then activated the RIPK1/Caspase 8-dependent apoptosis signaling pathway to cause neuronal death. EPZ5676 treatment was able to protect against ischemic neuronal death by inhibiting RIPK1-mediated apoptosis in mice brains following ischemic stroke. Because of the specific activation of Dot1L in cerebral ischemia, we suggest further studies to explore its feasibility as a potential therapeutic target for neuroprotection.

Supplementary Material

Table S1
Figures S1–S5
References 36–44

REFERENCES

1. Wang W, Jiang B, Sun H, Ru X, Sun D, Wang L, Wang L, Jiang Y, Li Y, Wang Y, et al. Prevalence, incidence, and mortality of stroke in China: results from a nationwide population-based survey of 480 687 adults. *Circulation*. 2017;135:759–771. doi: 10.1161/CIRCULATIONAHA.116.025250

2. Fan WY, Dai YQ, Xu HC, Zhu XM, Cai P, Wang LX, Sun CG, Hu CL, Zheng P, Zhao BQ. Caspase-3 modulates regenerative response after stroke. *Stem Cells*. 2014;32:473–486. doi: 10.1002/stem.1503

3. Nakagomi T, Takagi T, Beppu M, Yoshimura S, Matsuyama T. Neural regeneration by regionally induced stem cells within post-stroke brains: novel therapy perspectives for stroke patients. *World J Stem Cells*. 2019;11:452–463. doi: 10.4252/wjsc.v11.i8.452

4. Ashkenazi A, Dixit VM. Death receptors: signaling and modulation. *Science*. 1998;281:1305–1308. doi: 10.1126/science.281.5381.1305

5. Ea CK, Deng L, Xia ZP, Pineda G, Chen ZJ. Activation of IKK by TNFalpha requires site-specific ubiquitination of RIP1 and polyubiquitin binding by NEMO. *Mol Cell*. 2006;22:245–257. doi: 10.1016/j.molcel.2006.03.026

6. Li HX, Kobayashi M, Blonska M, You Y, Lin X. Ubiquitination of RIP is required for tumor necrosis factor alpha-induced NF-kappa B activation. *J Biol Chem*. 2006;281:13636–13643. doi: 10.1074/jbc.M600620200

7. Wright A, Reiley WW, Chang M, Jin W, Lee AJ, Zhang MY, Sun SC. Regulation of early wave of germ cell apoptosis and spermatogenesis by deubiquitinating enzyme CYLD. *Dev Cell*. 2007;13:705–716. doi: 10.1016/j.devcel.2007.09.007

8. Hitomi JI, Christofferson DE, Ng A, Yao JH, Degterev A, Xavier RJ, Yuan JY. Identification of a molecular signaling network that regulates a cellular necrotic cell death pathway. *Cell*. 2008;135:1311–1323. doi: 10.1016/j.cell.2008.10.044

9. Jones PA, Issa JPJ, Baylin S. Targeting the cancer epigenome for therapy. *Nat Rev Genet*. 2016;17:630–641. doi: 10.1038/nrg.2016.93

10. Feng Q, Wang HB, Ng HH, Erdjument-Bromage H, Tempst P, Struhl K, Zhang Y. Methylation of H3-lysine 79 is mediated by a new family of HMTases without a SET domain. *Curr Biol*. 2002;12:1052–1058. doi: 10.1016/S0960-9822(02)00901-6

11. Steger DJ, Lefterova MI, Ying L, Stonestrom AJ, Schupp M, Zhuo D, Vakoc AL, Kim JE, Chen JJ, Lazar MA, et al. DOT1L/KMT4 recruitment and H3K79 methylation are ubiquitously coupled with gene transcription in mammalian cells. *Mol Cell Biol*. 2008;28:2825–2839. doi: 10.1128/MCB.02076-07

12. Barski A, Cuddapah S, Cui KR, Roh TY, Schones DE, Wang ZB, Wei G, Chepelev I, Zhao KJ. High-resolution profiling of histone methylations in the human genome. *Cell*. 2007;129:823–837. doi: 10.1016/j.cell.2007.05.009

13. Mohan M, Herz HM, Takahashi YH, Lin CQ, Lai KC, Zhang Y, Washburn MP, Florens L, Shilatifard A. Linking H3K79 trimethylation to Wnt signaling through a novel Dot1-containing complex (DotCom). *Genes Dev*. 2010;24:574–589. doi: 10.1101/gad.1898410

14. Kim SK, Jung I, Lee H, Kang K, Kim M, Jeong K, Kwon CS, Han YM, Kim YS, Kim D, et al. Human histone H3K79 methyltransferase DOT1L protein binds actively transcribing RNA polymerase II to regulate gene expression (vol 287, pg 39698, 2012). *J Biol Chem*. 2013;288:295. doi: 10.1074/jbc.A112.384057

15. Chen CW, Koche RP, Sinha AU, Deshpande AJ, Zhu N, Eng R, Doench JG, Xu H, Chu SH, Qi J, et al. DOT1L inhibits SIRT1-mediated epigenetic silencing to maintain leukemic gene expression in MLL-rearranged leukemia. *Nat Med*. 2015;21:335–343. doi: 10.1038/nm.3832

16. Nassa G, Salvati A, Tarallo R, Gigantino V, Alexandrova E, Memoli D, Sellitto A, Rizzo F, Malanga D, Mirante T, et al. Inhibition of histone methyltransferase DOT1L silences ER alpha gene and blocks proliferation of antiestrogen-resistant breast cancer cells. Science. *Advances*. 2019;5:eaav5590. doi: 10.1126/sciadv.aav5590

17. McLean CM, Karemaker ID, van Leeuwen F. The emerging roles of DOT1L in leukemia and normal development. *Leukemia*. 2014;28:2131–2138. doi: 10.1038/leu.2014.169

18. Langley B, Brochier C, Rivieccio MA. Targeting histone deacetylases as a multifaceted approach to treat the diverse outcomes of stroke. *Stroke*. 2009;40:2899–2905. doi: 10.1161/STROKEAHA.108.540229

19. Suvarna NU, O'Donnell JM. Hydrolysis of N-methyl-D-aspartate receptor-stimulated cAMP and cGMP by PDE4 and PDE2 phosphodiesterases in primary neuronal cultures of rat cerebral cortex and hippocampus. *J Pharmacol Exp Ther*. 2002;302:249–256. doi: 10.1124/jpet.302.1.249

20. Gelderblom M, Leypoldt F, Steinbach K, Behrens D, Choe CU, Siler DA, Arumugam TV, Orthey E, Gerloff C, Tolosa E, et al. Temporal and spatial dynamics of cerebral immune cell accumulation in stroke. *Stroke*. 2009;40:1849–1857. doi: 10.1161/STROKEAHA.108.534503

21. Pasparakis M, Vandenabeele P. Necroptosis and its role in inflammation. *Nature*. 2015;517:311–320. doi: 10.1038/nature14191

22. Amin P, Florez M, Najafov A, Pan H, Geng J, Ofengeim D, Dziedzic SA, Wang H, Barrett VJ, Ito Y, et al. Regulation of a distinct activated RIPK1 intermediate bridging complex I and complex II in TNFalpha-mediated apoptosis. *Proc Natl Acad Sci USA*. 2018;115:E5944–E5953.

23. Vanden Berghe T, Linkermann A, Jouan-Lanhouet S, Walczak H, Vandenabeele P. Regulated necrosis: the expanding network of non-apoptotic cell death pathways. *Nat Rev Mol Cell Biol*. 2014;15:135–147. doi: 10.1038/nrm3737

24. Lork M, Verhelst K, Beyaert R. CYLD, A20 and OTULIN deubiquitinases in NF-kappab signaling and cell death: so similar, yet so different. *Cell Death Differ*. 2017;24:1172–1183. doi: 10.1038/cdd.2017.46

25. Hsieh J, Eisch AJ. Epigenetics, hippocampal neurogenesis, and neuropsychiatric disorders: unraveling the genome to understand the mind. *Neurobiol Dis*. 2010;39:73–84. doi: 10.1016/j.nbd.2010.01.008

26. Mehler MF. Epigenetic principles and mechanisms underlying nervous system functions in health and disease. *Prog Neurogibol*. 2008;86:305–341. doi: 10.1016/j.pneurobio.2008.10.001

27. Qureshi IA, Mehler MF. Emerging role of epigenetics in stroke: part 1: DNA methylation and chromatin modifications. *Arch Neurol*. 2010;67:1316–1322. doi: 10.1001/archneurol.2010.275

28. Min J, Feng Q, Li Z, Zhang Y, Xu RM. Structure of the catalytic domain of human DOT1L, a Non-set domain nucleosomal histone methyltransferase. *Cell*. 2003;112:711–723. doi: 10.1016/S0092-8674(03)00114-4

29. Lambertsen KL, Biber K, Finsen B. Inflammatory cytokines in experimental and human stroke. *J Cereb Blood Flow Metab*. 2012;32:1677–1698. doi: 10.1038/jcbfm.2012.88

30. Welchman RL, Gordon C, Mayer RJ. Ubiquitin and ubiquitin-like proteins as multifunctional signals. *Nat Rev Mol Cell Biol*. 2005;6:599–609.

31. Behrends C, Harper JW. Constructing and decoding unconventional ubiquitin chains. *Nat Struct Mol Biol*. 2011;18:520–528. doi: 10.1038/nsmb.2066

32. Tan JMM, Wong ESP, Kirkpatrick DS, Pletnikova O, Ko HS, Tay S-P, Ho MWL, Troncoso J, Gygi SP, Lee MK, et al. Lysine 63-linked ubiquitination promotes the formation and autophagic clearance of protein inclusions associated with neurodegenerative diseases. *Hum Mol Genet*. 2008;17:431–439. doi: 10.1093/hmg/ddm320

33. Walczak H. TNF and ubiquitin at the crossroads of gene activation, cell death, inflammation, and cancer. *Immunol Rev*. 2011;244:9–28. doi: 10.1111/j.1600-065X.2011.01066.x

34. Wang L, Du F, Wang X. TNF-alpha induces two distinct caspase-8 activation pathways. *Cell*. 2008;133:693–703. doi: 10.1016/j.cell.2008.03.036

35. Feoktistova M, Geserick P, Kellert B, Dimitrova DP, Langlais C, Hupe M, Cain K, MacFarlane M, Hacker G, Leverkus M. cIAPS block ripoptosome formation, a RIP1/caspase-8 containing intracellular cell death complex differentially regulated by cFLIP isoforms. *Mol Cell*. 2011;43:449–463. doi: 10.1016/j.molcel.2011.06.011

36. Han RQ, Ouyang YB, Xu LJ, Agrawal R, Patterson AJ, Giffard RG. Postischemic brain injury is attenuated in mice lacking the beta(2)-adrenergic receptor. *Anest Analg*. 2009;108:280–287. doi: 10.1213/ane.0b013e318187ba6b

37. Bederson JB, Pitts LH, Tsuji M, Nishimura MC, Davis RL, Bartkowski H. Rat middle cerebral artery occlusion: evaluation of the model and development of a neurologic examination. *Stroke*. 1986;17:472–476. doi: 10.1161/01.STR.17.3.472

38. Li Q, Cao Y, Dang C, Han B, Han R, Ma H, Hao J, Wang L. Inhibition of double-strand DNA-sensing cGAS ameliorates brain injury after ischemic stroke. *EMBO Mol Med*. 2020;12:e11002. doi: 10.15252/emmm.201911002

39. Zhao YJ, Nai Y, Ma QS, Song DJ, Ma YB, Zhang LH, Mi LX. Dl-3-n-butylphthalide protects the blood brain barrier of cerebral infarction by activating the Nrf-2/HO-1 signaling pathway in mice. *Eur Rev Med Pharmacol Sci*. 2018;22:2109–2118. doi: 10.26355/eurrev_201804_14744

40. Deng XX, Li SS, Sun FY. Necrostatin-1 prevents necroptosis in brains after ischemic stroke via inhibition of RIPK1-mediated RIPK3/MLKL signaling. *Aging Dis*. 2019;10:807–817. doi: 10.14336/AD.2018.0728

41. Ye ZY, Xing HY, Wang B, Liu M, Lv PY. Dl-3-n-butylphthalide protects the blood-brain barrier against ischemia/hypoxia injury via upregulation of tight junction proteins. *Chin Med J (Engl)*. 2019;132:1344–1353. doi: 10.1097/CM9.0000000000000232

42. Pan Q, He C, Liu H, Liao X, Dai B, Chen Y, Yang Y, Zhao B, Bihl J, Ma X. Microvascular endothelial cells-derived microvesicles imply in ischemic stroke by modulating astrocyte and blood brain barrier function and cerebral blood flow. *Mol Brain*. 2016;9:63. doi: 10.1186/s13041-016-0243-1

43. Liu Q, Qiu J, Liang M, Golinski J, van Leyen K, Jung JE, You Z, Lo EH, Degterev A, Whalen MJ. Akt and mTOR mediate programmed necrosis in neurons. *Cell Death Dis*. 2014;5:e1084. doi: 10.1038/cddis.2014.69

44. Yang DI, Wei G, Long F, Nie H, Tian X, Qu L, Wang ShuangXi, Li P, Qiu Y, Wang Y, et al. Histone methyltransferase Smyd3 is a new regulator for vascular senescence. *Aging Cell*. 2020;19:e13212. doi: 10.1111/acel.13212

SUPPLEMENTAL MATERIAL

Data S1.

Supplemental Methods

Materials

EPZ5676 (Dot1L inhibitor) was purchased from Selleckchem (Selleck, USA). 2,3,5-triphenyltetrazolium chloride (TTC) was purchased Sigma (Sigma-Aldrich, USA).

Animal studies

Male C57BL/6J mice (22-25 g) were randomly divided into three groups: sham-operated group (Sham); middle cerebral artery occlusion (MCAO) group (MCAO); and an EPZ5676-treated group (MCAO+EPZ5676). Mice were kept anesthetized during surgery with 1% pentobarbital sodium (50 mg/kg, i.p, Sigma). Transient ischemia was induced by using the suture occlusion technique, as previously described [37], with minor modifications. The common carotid artery area was exposed, and a silicon rubber-coated filament of size 6-0 was inserted through the left internal carotid artery until the approximate branch of the left middle cerebral artery (MCA) and left in place for 90 min to block blood flow. Subsequently, the suture and the filament were removed to allow reperfusion for 24 hr and wounds were sutured. For sham animals, the filament was advanced to the MCA and withdrawn immediately. Mice were prescreened to select those in line with the criteria described as Bederson [38]. EPZ5676 (20 mg/kg) was administered by intraperitoneal (i.p.) injection daily for 7 days before MCAO.

Similarly, the Sham-operated and MCAO groups received equal volumes of physiological saline.

HT22 cell culture

Immortalized hippocampal neuroblasts (HT22, ATCC) were incubated in DMEM-F12 supplemented with 10% FBS at 37°C in a humidified atmosphere with 5% CO_2.

Assessment of brain edema

Mice were sacrificed and the brain was quickly decapitated and taken under low temperature. The photos were taken to observe the brain edema.

Assessment of cerebral infarction volume

TTC staining was used to evaluate infarct size [39]. At 24 hr after operation, the mice were sacrificed after anesthesia, and their brains were quickly and completely removed. The olfactory bulbs and cerebellums were excised, and the brains were continuously and equidistantly cut into 5 coronal sections. The brain slices were completely immersed in 1% TTC solution and incubated at 37°C for 30 min. TTC was discarded after staining. Then, the brain slices were fixed in 4% paraformaldehyde for 24 hr and placed in order [40]. After that, sections were photographed and the infarcted regions in each section were evaluated by using *Image J* software. The percentage of the infarct volume was calculated by the following formula: [(total contralateral hemispheric volume)-(total ipsilateral hemispheric stained volume)]/(total contralateral hemispheric volume) × 100% [41].

Evans blue (EB) dye leakage assay

The integrity of the BBB was evaluated with a modified Evans blue extravasation

method as previously reported [42]. After anesthesia with pentobarbital sodium (50 mg/kg, intraperitoneal injection), 37°C warmed Evans blue dye (2%, 4 mL/kg) was injected into the femoral vein and allowed to circulate for 2 h. This was followed by perfusion with phosphate-buffered saline (PBS) via the aorta to wash out any remaining dye in the blood vessels. Then, use a digital camera to take pictures of the whole brain and coronal section to observe the size and extent of the EB stained area.

Measurement of cerebral blood flow (CBF)

24 hr after stroke, the CBF of mice from various groups was determined by the PeriCam PSI System (primed, Sweden) as previously described [43]. Briefly, the mouse was anesthetized with 1% pentobarbital sodium and placed on a stereotaxic apparatus. A crossing skin incision was made on the head to expose the whole skull. PeriCam PSI System scanning (2.0 × 1.4 cm) was performed on the intact skull for approximately 1 min. The mean blood perfusion of the ischemic hemisphere was analyzed with the software (Pimsoft).

Small interfering RNA (siRNA) transfection *in vitro*

Cells were plated in six-well culture dishes and were transfected with Dot1L and Control small interfering RNA (siRNA) (GenePharma Co. Ltd. Shanghai, China) using Lipofectamine RNA iMAX (ThermoFisher Scientific) according to the manufacturer's instructions. The sequences are as follows: Dot1L siRNA: 5'-GCAGAGGCUGUGUGACAAATT-3' and the scrambled siRNA: 5'-UUCUCCGAACGUGUCACGUTT-3'. Experiments were performed 24 hr after transfection.

Assessment of Caspase 3 activity

Caspase 3 activity was detected using the Caspase 3 activity kit (Meilunbio, China) according to the manufacturer's instructions.

Immunohistochemical staining

Tissues sections were treated with autoclaving at 121°C for 15 min in 0.01 mol/L citrate-buffered saline (pH 6.0) for antigen retrieval. The sections were then immersed in 3% H_2O_2 for 30 min at room temperature to block the endogenous peroxidase activity. After deactivation, 10% normal goat serum was used to block nonspecific binding of the immunological reagents. After incubation of the antibodies against iNOS or CD45 at 4°C overnight, each slide was rinsed three times in PBS and incubated with biotinylated anti-mouse IgG and HRP-streptavidin at room temperature according to the immunohistochemical staining kit (Beyotime Biotechnology), stained with DAB substrate. Finally, nuclear counterstaining was done using hematoxylin.

Immunofluorescence staining

After the stimulation as indicated, cells were fixed with pre-warmed 4% paraformaldehyde and then permeabilized for 10 min using 1% Triton X-100 in dissolved in PBS followed by incubation with the primary antibodies at 4°C overnight. The cells were washed three times with PBS and incubated with Fluor-conjugated secondary antibody (Invitrogen). The nucleus was stained with 4',6-diamidino-2-phenylindole (DAPI) to locate the cell. Fluorescent pictures were obtained with a Zeiss fluorescence microscope.

Western blot analysis

Tissue samples from the left ischemic hemisphere or culture cells were pooled and homogenized with a homogenizer or by sonication in ristocetin-induced platelet aggregation (RIPA) buffer containing protease and phosphatase inhibitors (Complete Protease Inhibitor Cocktail and PhosSTOP Phosphatase Inhibitor Cocktail; both from Roche), and then centrifuged at 12,000 g for 10 min at 4°C. The supernatant was collected. The total protein concentration in each sample was determined with a bicinchoninic acid (BCA) assay (QuantiPro BCA Assay Kit, Sigma-Aldrich) according to the manufacturer's instructions. Equal amount of protein samples was separated by SDS-polyacrylamide gel electrophoresis and transferred to nitrocellulose membranes (Millipore). The membranes were blocked with 5% skimmed milk (wt/vol) in Tris-buffered saline supplemented with 0.1% Tween 20 (TBST) for 1 hr at room temperature and then incubated with the corresponding primary antibodies: rabbit anti-VCAM-1 (1:1000; Proteintech); rabbit anti-COX-2 (1:1000; Proteintech); rabbit anti-iNOS (1:1000; Cell Signal Technology); rabbit anti-Zona Occludens-1 (ZO-1, 1:1000; Proteintech); rabbit anti-Claudin-1 (1:1000; Proteintech); rabbit anti-Bax (1:500; Cell Signaling Technology); rabbit anti-Bcl-2 (1:500; Cell Signaling Technology); rabbit anti-PARP1 (1:1000; Proteintech); rabbit anti-Caspase 3 (1:1000; Cell Signaling Technology); rabbit anti-RIPK1 (1:1000; Proteintech); rabbit anti-RIPK3 (1:1000; Proteintech); rabbit anti-Caspase 8 (1:1000; Proteintech); rabbit anti-Dot1L (1:1000; Abclonal); rabbit anti-H3K79me3 (1:1000; Cell Signaling Technology); rabbit anti-K63 (1:1000; Cell Signaling Technology); rabbit anti-Total-H3 (1:1000; Cell Signaling Technology); rabbit anti-A20 (1:1000; Proteintech); rabbit anti-CYLD (1:1000;

Proteintech); rabbit anti-cIAP1 (1:1000; Proteintech); mouse anti-Caspase 9 (1:1000; Proteintech); mouse anti-p53 (1:1000; Proteintech); and mouse anti-GAPDH (1:20000; Proteintech) at 4°C overnight. The members were then washed and incubated for 1 hr at room temperature with the speciesappropriate horseradish peroxidase (HRP)-labeled secondary antibody (1:5000; Jackson ImmunoResearch Inc., USA). Protein-specific signals were detected using a Bio-Rad Imager (Bio-Rad, Hercules, CA, USA), and the bands were quantified by densitometric analysis (ImageJ software, NIH). The relative amounts of proteins were normalized against GAPDH.

RNA extraction and quantitative real-time polymerase chain reaction (qRT-PCR)

Total RNA was isolated from the cells or tissues using TRIzol reagent (Takara Bio Inc., China). Reverse transcription was performed according to the instruction of the Prime RT Master Mix kit (Takara Bio Inc., China). Quantitative real-time PCR was performed in triplicate using SYBR Premix EX Taq II (Yeasen Biotech Co., Ltd. China). The sequences of primers were shown in **Table S1**.

Co-immunoprecipitation

For co-immunoprecipitation experiments, HT22 cells were treated with OGD/R in the presence or absence of EPZ5676 (20 µmol/L) for 4 h, and were collected, washed in PBS and lysed in a buffer containing 20 mmol/L Tris-HCl (pH 8), 137 mmol/L NaCl, 10% glycerol, 1% Nonidet P-40 (NP-40), 2 mmol/L EDTA, and protease inhibitor cocktail. Precleaning was achieved with 50 mL of protein A/G agarose beads (Santa Cruz, Dallas, TX, USA) for 1 hr, and lysates were incubated overnight at 4°C in presence of 50 mL of protein A/G agarose or magnetic beads and 1-2 mg rabbit anti-

RIPK1 or rabbit anti-Caspase 8 antibody before analysis by western blotting. The same amount of irrelevant mouse IgG (Santa Cruz) was used to control for nonspecific IgG binding to RIPK1 or Caspase 8 [44].

ChIP-PCR

ChIP assays was performed as described previously [45]. Briefly, the cells were fixed with 1% formaldehyde for 10 min, then neutralized with 0.125 mM glycine. Then, the samples were sheared with sonication. DNA samples were isolated after immunoprecipitation with the specific H3K79me3 (Cell Signaling Technology) and a rabbit IgG (Santa Cruz) antibodies. Normal PCR was applied to quantify precipitated DNA using rat Tnfaip3 (A20) promoter-specific primers (Forward: 5'-CAAGCCTGAGGTCCTGTGTG-3'; Reverse: 5'-CGGAGAAACTCCTAGGTCCCG-3'), rat Cyld promoter-specific primers (Forward: 5'-TTCTCTGGATCGCTTCCCAC-3'; Reverse: 5'-GATGGCTGATTGGGCGAAAG-3'), rat Bric2 (cIAP1) promoter-specific primers (Forward: 5'-GAACTCACAGGCTGCACATC-3'; Reverse: 5'-AGGGTGAAAACCAGACGCAC-3').

Table S1. Primers used for qRT-PCR validation.

Gene name	Primer name	Primer sequence (5´ to 3´)
Dot1L	Rat _Dot1L_F	CAAAGTCCCTGAGAGCAAGG
	Rat _Dot1L_R	TGGCAGCACTCATTTTCTTG
GAPDH	Rat _GAPDH_ F	TCAACGGCACAGTCAAGG
	Rat _GAPDH_ R	AGCATCAAAGGTGGAAGAAT
Cox-2	Rat _Cox-2_F	TGCATTCTTTGCCCAGCACT
	Rat _Cox-2_R	AAAGGCGCAGTTTACGCTGT
Nos2	Rat _Nos2_F	CAGCCTGTGAGACGTTCGAT
	Rat _Nos2_R	CCCATGTTGCGTTGGAAGTG
p53	Rat _p53_F	GACGGGACAGCTTTGAGGTT
	Rat _p53_R	CTCCGGGCAATGCTCTTCTT
Vcam-1	Rat _Vcam-1_F	CTGCACGGTCCCTAATGTGT
	Rat _Vcam-1_R	CAAGAGCTTTCCCGGTGTCT
Bax	Rat _Bax_F	AGGACGCATCCACCAAGAAG
	Rat _Bax_R	CAGTTGAAGTTGCCGTCTGC
CLDN1	Mouse _CLDN1_F	TATGACCCCTTGACCCCCAT
	Mouse _CLDN1_R	AGAGGTTGTTTTCCGGGGAC
Tjp1	Mouse _Tjp1_F	CTCTTGCTGGCCCTAAACCT
	Mouse _Tjp1_R	TTCGGGTGGCTTCACTTGAG
Ripk1	Mouse _Ripk1_F	AGGAAGCATACCCACCATGC

	Mouse _Ripk1_R	TGGTGGTTGTGAACTCGGTC	**T**
Ripk3	Mouse _Ripk3_ F	CTTGGTACACCTGGAACGCA	
	Mouse _Ripk3_ R	GGGAAAGGCAGTTCTCGGTT	
Caspase 8	Mouse _Caspase 8_ F	ACAGGGTCATGCTTCTTCGG	
	Mouse _Caspase 8_ R	GCAGGCTCTTGTTGACTTGC	
Tnfaip3	Mouse _Tnfaip3_ F	TGCCTTCAGGATGTCACTCG	
	Mouse _Tnfaip3_ R	CAGACTTGGAGCGTTGGTGA	
Cyld	Mouse _Cyld_ F	ATTAGCGGAGAGGACGGTGT	
	Mouse _Cyld_ R	CCCCATCCGTGAAACCTTGA	
Birc2	Mouse _Birc2_ F	CATTGGAAGAGCAGTTGCGG	
	Mouse _Birc2_ R	GCAGATGGGGCACTTCCTTA	
GAPDH	Mouse _GAPDH_ F	CTTCTCTTGTGACAAAGTGGACAT	
	Mouse _GAPDH_ R	TTCTCAGCCTTGACTGTGCC	

Figure S1. Expression of Dot1L increases in cortical neurons after OGD and in brain of mice after MCAO.
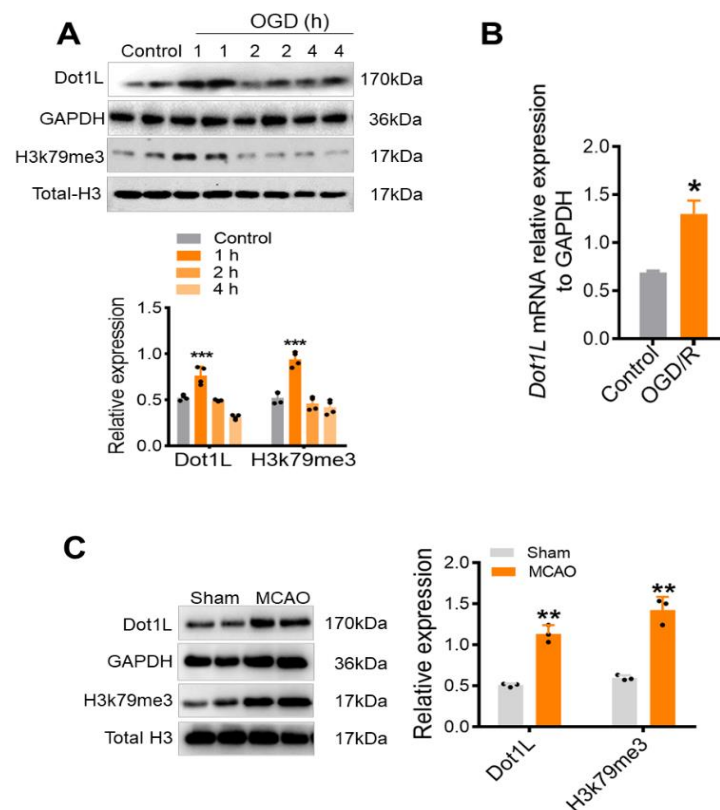
(**A**) Expression of Dot1L increases in cortical neurons after OGD. OGD-reoxygenation (in vitro ischemic model) induces expression of Dot1L and H3K79me3 in dedicated time. Upper panel shows real-time Dot1L and H3K79me3 expression in cortical neurons after OGD. Lower panel demonstrates densitometric analyses of four independent experiments; (**B**) OGD prominently stimulates mRNA expression of Dot1L. Cortical neurons were treated with OGD 1 hr and 24 hr of reoxygenation. Data are presented as mean ± S.D of three independent experiments, $^*p < 0.05$, $^{***}p < 0.001$ compared with Control. (**C**) Immunoblot analysis of Dot1L and H3K79me3 in brain of mice after MCAO; data shown are presented as mean ± S.D from at three independent replicates for 6-10/group, $^{**}p < 0.01$. The data is analyzed and counted through Anova or T-test.

Figure S2. EPZ5676 reduces inflammation response.
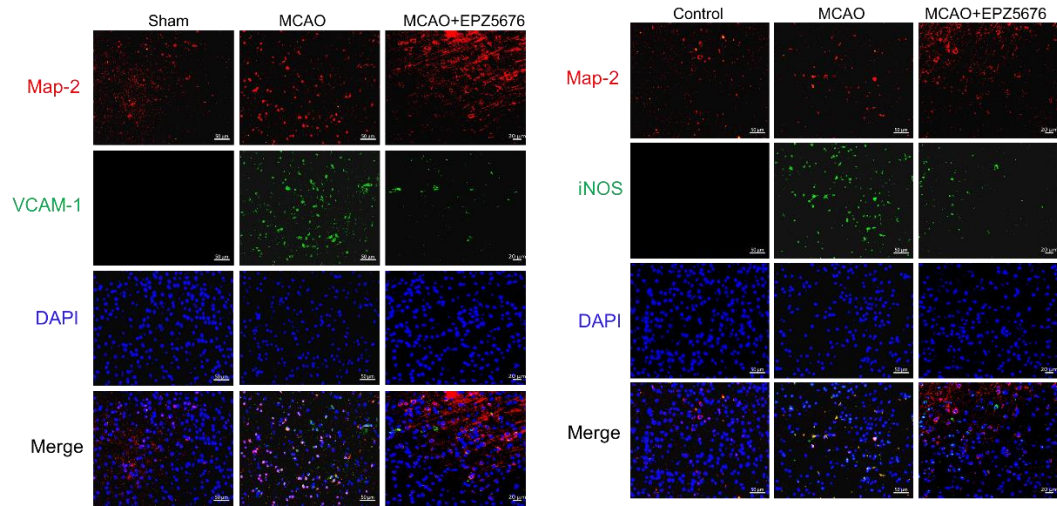
Representative images of immunofluorescence microscopy of VCAM-1, iNOS and Map-2 in MCAO mice. Scale bars: 20 μm.

Figure S3. Mice lacking Dot1L reduces apoptosis and inflammation response, promotes intercellular links.
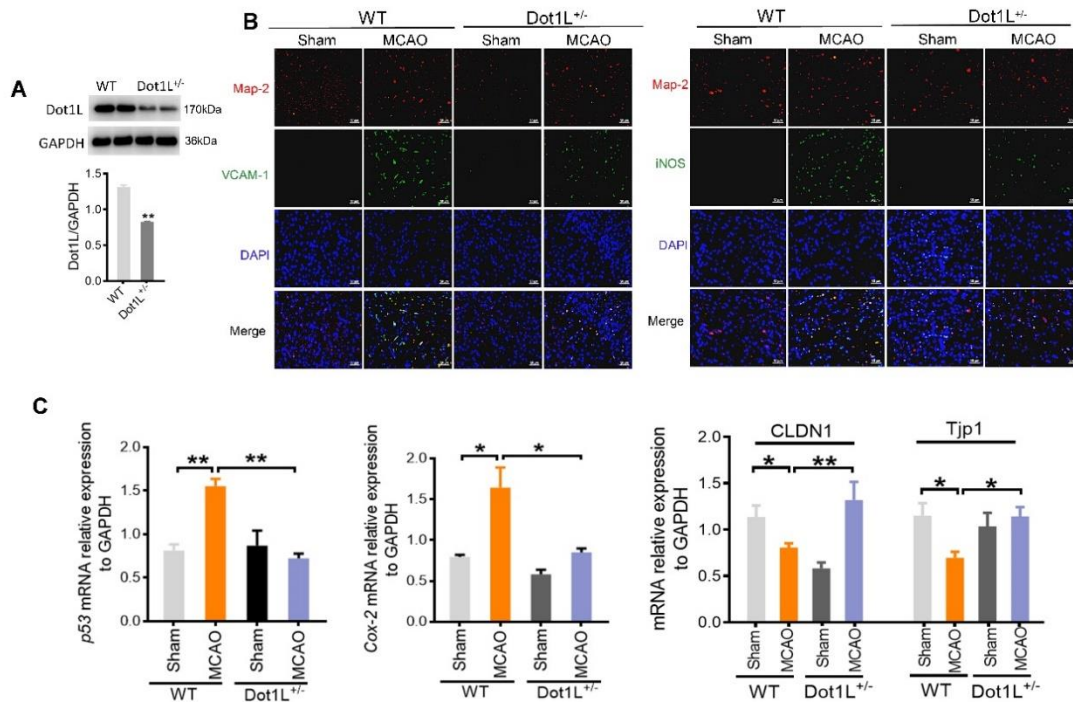
(**A**) Immunoblot analysis of Dot1L protein expression in brain of WT and Dot1L$^{+/-}$ mice. Data shown are presented as mean ± S.D for 6-10/group, $^{**}p < 0.01$ compared with WT mice. (**B**) Immunofluorescence staining of VCAM-1, iNOS and Map-2 in brain of WT and Dot1L$^{+/-}$ mice after MCAO. Scale bars: 20 μm. (**C**) qRT-PCR to quantify mRNA level of p53, Cox-2, CLDN1, and Tjp1. All data are presented as mean ± S.D; n=6/group, $^{*}p < 0.05$, $^{**}p < 0.01$. The data is analyzed and counted through Anova or T-test.

Figure S4. Suppression or knockdown of Dot1L reduces cortical neuronal apoptosis and inflammation response after OGD.
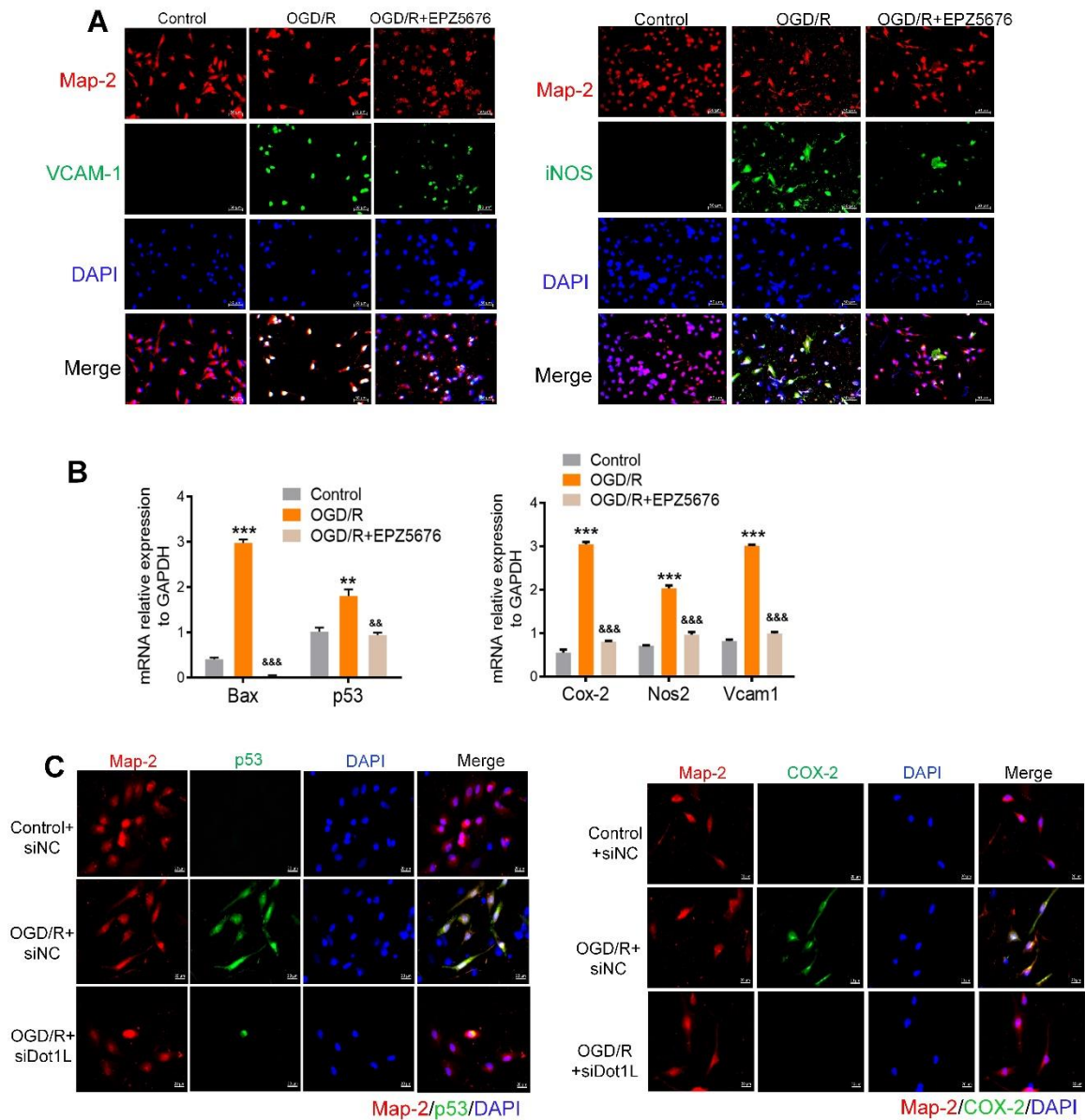
Rat neocortical neurons were pre-treated with 20 μM EPZ5676 for 4 h and subsequently treated with OGD 4 hr and 24 hr of reoxygenation. Immunofluorescence staining of Map-2 and VCAM-1 or iNOS in cortical neurons after OGD. Scale bars: 20 μm (**A**); qRT-PCR to quantify mRNA level of p53, Bax, Cox-2, Nos2, and Vcam-1. All data are presented as mean ± S.D of four independent experiments, $^{**}p < 0.01$, $^{***}p <$

0.001 compared with Control, $^{\&\&}p < 0.01$, $^{\&\&\&}p < 0.001$ compared with OGD/R. The data is analyzed and counted through Anova or T-test (**B**). (**C**) Rat neocortical neurons were transfected with either control siRNA (siNC) or Dot1L siRNA (siDot1L) cultured for 48 h and subsequently treated with OGD/R, Immunofluorescence staining of Map-2 and p53 or COX-2 in cortical neurons. Scale bars: 20 µm.

Figure S5. Suppression of Dot1L reduces HT22 cell apoptosis and inflammation response after OGD.
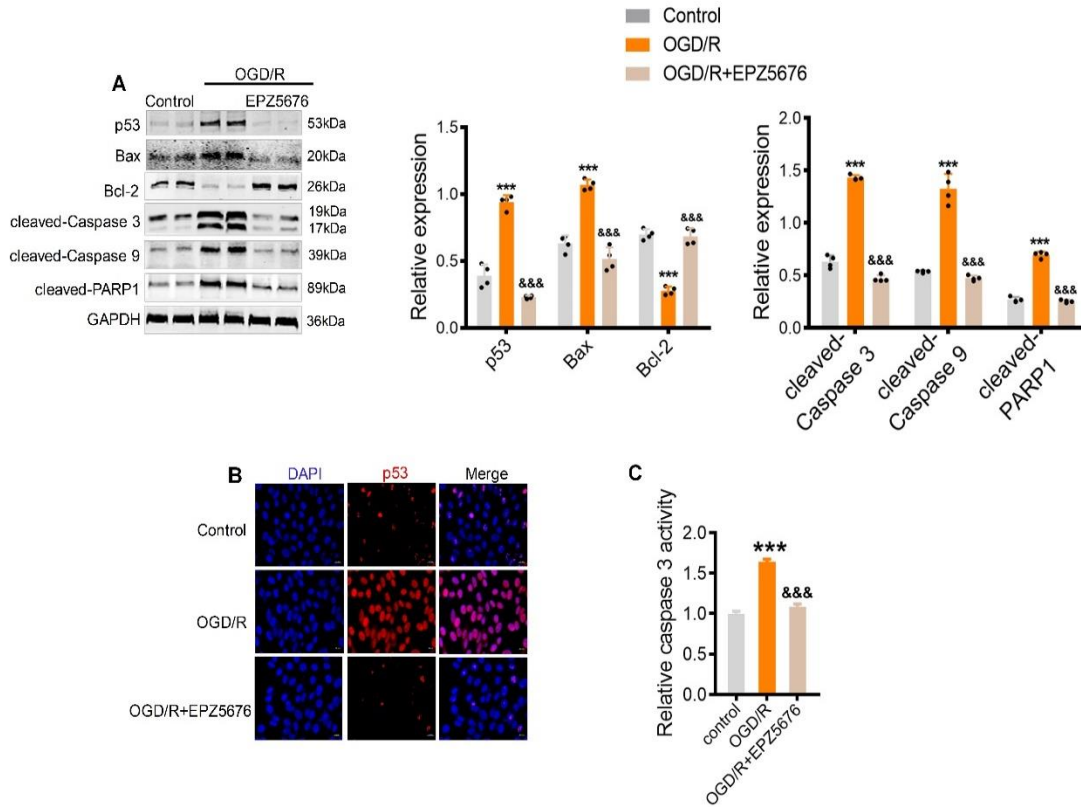
HT22 cell were pre-treated with 20 μM EPZ5676 for 4 h and subsequently treated with OGD 4 hr and 24 hr of reoxygenation. Immunoblot analysis of apoptosis-related proteins (Bax, Bcl-2, p53, cleaved-PARP1, cleaved-Caspase 3, cleaved-Caspase 9) (**A**); Immunofluorescence staining of p53 in cortical neurons after OGD. Scale bars: 20 μm (**B**); Caspase 3 activity was assayed (C). All data are presented as mean ± S.D of four independent experiments, [***]$p < 0.001$ compared with Control, [&&&]$p < 0.001$ compared with OGD/R. The data is analyzed and counted through Anova or T-test.